Magnetic and Charge Dynamics in a Doped One-Dimensional Transition Metal Oxide

J. F. DiTusa,[1] S-W. Cheong,[1] J.-H. Park,[1] G. Aeppli,[1] C. Broholm,[2] and C. T. Chen[1]
[1]*AT&T Bell Laboratories, Murray Hill, New Jersey 07974*
[2]*Department of Physics and Astronomy, Johns Hopkins University, Baltimore, Maryland 21218 and National Institute of Standards and Technology, Gaithersburg, Maryland 20899*
(Received 22 November 1993; revised manuscript received 29 April 1994)

We have measured the electrical resistivity, polarized x-ray absorption, and magnetic neutron scattering for $Y_{2-x}Ca_xBaNi_{1-y}Zn_yO_5$ to determine how doping affects the charge and spin dynamics of a Haldane chain compound. While Zn doping, which severs the NiO chains, increases the resistivity beyond that of the pure material, Ca doping introduces holes, residing mainly in the $2p_z$ orbital of the oxygens in the NiO chains. Both dopants lead to simple finite size effects above the Haldane gap. In addition, we have discovered that Ca doping yields substantial magnetic states below the Haldane gap.

PACS numbers: 75.25.+z, 71.30.+h, 72.80.Ga

Doping of two- and three-dimensional (3D) transition metal oxides yields phenomena ranging from strongly renormalized Fermi liquid behavior in the vanadates to high temperature superconductivity in the cuprates [1,2]. In view of the enhanced quantum fluctuations in 1D systems, doping of transition metal chain oxides could well lead to equally surprising discoveries. Furthermore, because the theory of 1D systems is less speculative than that of 2D and 3D materials, tests of theory should be simpler than for the cuprates and vanadates. Thus motivated, we have performed transport, x-ray absorption, and neutron scattering experiments to determine how doping affects Y_2BaNiO_5, a charge transfer insulator [3] containing Ni^{2+} ($S = 1$) chains with a quantum disordered, Haldane ground state [4–7]. To the best of our knowledge these experiments are the first on any carrier-doped 1D transition metal oxide, and Y_2BaNiO_5 provides the first gapped spin liquid, of any dimension, to which carriers can be added. The key result is that while substitution of nonmagnetic Zn^{2+} for magnetic Ni^{2+} on the chains simply produces effects one can associate with chain cutting, replacing the *off-chain* Y^{3+} by Ca^{2+} has far more dramatic consequences. In particular, holes appear in oxygen orbitals along the NiO chains radically changing the temperature dependence of the resistivity from the simple insulating behavior of the parent. In both the parent and doped compounds, electrical conduction is 1D. Carrier doping also yields new magnetics states below the Haldane gap.

The specimens were large (~5 cm^3) polycrystalline pellets as well as small ($0.5 \times 1.0 \times 3.0$ mm^3) single crystals. We prepared the pellets using a standard solid state reaction, while we grew the crystals from Ba- and Ni-rich melts [8–10]. The stoichiometry of Y, Ca, Ba, Zn, and Ni in each of these samples was determined by analysis of the γ rays produced upon cold neutron capture at the National Institute of Standards and Technology (NIST) research reactor. All four pellets had compositions in agreement with the nominal values. The magnetic susceptibilities of the pellets were consistent with those obtained previously for the same compositions [8,11].

Figure 1 displays the four-terminal dc resistivity (ρ) [12] for single crystals with silver paste contacts. The conduction in pure Y_2BaNiO_5 is remarkably 1D with ρ along the chain (a axis) 3 orders of magnitude lower than that perpendicular to the chains. The activated form, $\rho = \rho_0 e^{\Delta_g/2k_BT}$, gives an excellent account of the temperature (T) dependent ρ of the nominally pure samples. Fits by this form give $\Delta_g = 600$ meV, which is independent of crystallographic direction. This transport gap is significantly smaller than the expected intrinsic gap of ~2 eV [13], most likely due to impurities or oxygen defects.

Ca and Zn doping affect ρ in dramatically different ways. Zn substitution increases ρ along the chain axis.

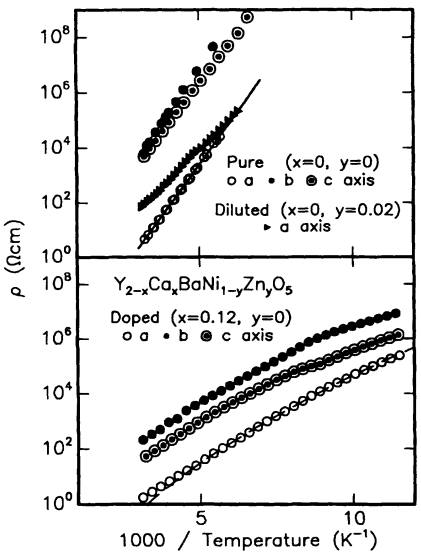

FIG. 1. Plot of the resistivity for single crystals of $Y_{2-x}Ca_xBaNi_{1-y}Zn_yO_5$. Solid line (top frame) corresponds to a transport gap of $\Delta_g = 600$ meV. Dashed line (lower frame) through data for Ca diluted single crystal a-axis resistivity is a fit by variable range hopping form in text.

0031-9007/94/73(13)/1857(4)$06.00

This is consistent with strong carrier scattering from the impurities inserted into the chains along which conduction occurs. In contrast, Ca doping greatly lowers ρ while preserving the 1D nature of the conduction. Furthermore, simple thermal activation across a barrier no longer describes $\rho(T)$. Indeed, the effective barrier Δ_g decreases as the temperature is lowered, consistent with variable range hopping, which in 1D yields $\rho = \rho_0 \exp\sqrt{T_0/T}$ [14]. For the $x = 0.12$ sample used to obtain the data in the lower part of Fig. 2, the best fit (dashed line) to the a-axis resistivity yields $\rho_0 = 1.0 \times 10^{-12}$ Ω cm and $T_0 = 4.5$ eV. We conclude that Ca substitution has added carriers to the NiO chains not found with Zn dilution. The carriers do not induce clean metallic behavior, which is not surprising for a 1D material where an arbitrarily small concentration of defects leads to localization. Y_2BaNiO_5 thus becomes a new member of the very small group [15] of effectively 1D conductors, and of course the first one whose insulating parent has a spin liquid ground state [6,7].

Having demonstrated that carriers are essentially constrained to move parallel to the NiO chains, we set out to determine their microscopic nature by polarized x-ray absorption spectroscopy (XAS). O K-edge and Ni L-edge polarized fluorescence yield XAS spectra were taken using the AT&T Bell Laboratories Dragon soft-x-ray beam line at the Brookhaven National Synchrotron Light Source. The experimental configuration is similar to that used previously for $La_{2-x}Sr_xCuO_4$ [16]. Since the chain direction is in the sample surface plane, a normal incidence geometry was utilized.

Figure 2(a) shows the O K-edge region of the XAS spectra of two $Y_{2-x}Ca_xBaNiO_5$ single crystals taken

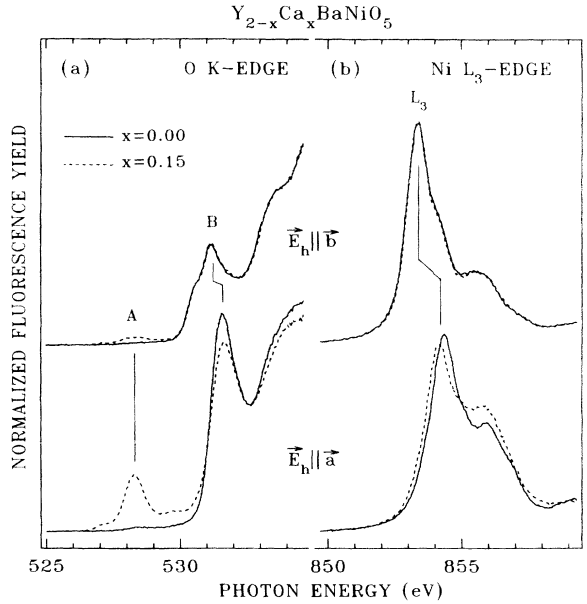

FIG. 2. Oxygen K-edge (left frame) and Ni L_3-edge (right frame) polarized fluorescence yield x-ray absorption spectra for Y_2BaNiO_5 (solid line) and $Y_{1.9}Ca_{0.1}BaNiO_5$ (dashed line).

with two polarization geometries, i.e., $\mathbf{E}_h \| \mathbf{a}$ and $\mathbf{E}_h \| \mathbf{b}$. Similar to other doped charge-transfer compounds, two distinct prepeaks were observed. Prepeak B corresponds to the transition from the O $1s$ level to states with O $2p$ character in the upper Hubbard band, and prepeak A is due to the transition to the doping induced O $2p$ states at the top of the valence band [16]. Since the intensity increase of prepeak A in the $\mathbf{E}_h \| \mathbf{a}$ spectra with Ca doping is an order of magnitude larger than that in the $\mathbf{E}_h \| \mathbf{b}$ spectra, the doping induced holes must have mainly the O $2p_z$ character (here we use z, x, and y to denote the a, b, and c crystal axis, respectively). A spectral weight transfer from prepeak B to A is also observed in the $\mathbf{E}_h \| \mathbf{a}$ spectra, in agreement with what is found in other doped charge transfer insulators such as $La_{2-x}Sr_xCuO_4$ [16].

Figure 2(b) shows the Ni L_3 XAS. Upon Ca doping, the $\mathbf{E}_h \| \mathbf{a}$ spectra exhibit noticeable changes, e.g., an energy shift and spectral weight transfer, while the $\mathbf{E}_h \| \mathbf{b}$ spectra are essentially intact. The rather complicated line shape is due to the multiplet structure associated with Ni $2p_{3/2}$ to $3d$ transitions. Most of the intensity in both spectra derives from the $\underline{3d}_{3z^2-r^2}\underline{3d}_{x^2-y^2} \rightarrow \underline{2p}_{3/2}\underline{3d}_{x^2-y^2}$ and $\underline{3d}_{3z^2-r^2}\underline{3d}_{x^2-y^2} \rightarrow \underline{2p}_{3/2}\underline{3d}_{3z^2-r^2}$ transitions, respectively. This is consistent with the similarity in the L_3 white line intensities observed for $\mathbf{E}_h \| \mathbf{a}$ and $\mathbf{E}_h \| \mathbf{b}$. The 0.91 eV shift toward lower energy in the L_3 white line, found on going from $\mathbf{E}_h \| \mathbf{a}$ to $\mathbf{E}_h \| \mathbf{b}$, is the $\underline{3d}_{x^2-y^2}/\underline{3d}_{3z^2-r^2}$ crystal field splitting. In contrast to the prepeak in the oxygen absorption spectrum, the intensity of the Ni L_3 white line does not increase with Ca doping, suggesting that the doping induced holes have more O $2p_z$ character than Ni $3d_{3z^2-r^2}$ character.

Our transport and x-ray absorption measurements show that $Y_{2-x}Ca_xBaNiO_5$ is indeed the first 1D analog of the much-studied 2D copper and nickel oxides. It is well known that doping has as profound an influence on the magnetism as on the charge fluctuations of the latter compounds. To see whether doping has a similarly dramatic effect on the spin correlations in Y_2BaNiO_5, we have performed inelastic neutron scattering experiments on $Y_{2-x}Ca_xBaNiO_5$ for $x = 0.04$ and 0.10. For reference, we have also examined pure Y_2BaNiO_5 and $Y_2BaNi_{1-y}Zn_yO_5$ with $y = 0.04$, where Zn simply cuts the NiO chains. The instrument used was the BT2 thermal neutron triple axis spectrometer at NIST. We performed energy scans with a fixed final neutron energy of 14.7 meV with collimations of 60′-20′ and 42′-93′ around the pyrolytic graphite (PG) (002) monochromator and analyzer, respectively. For constant energy scans as a function of wave vector (q) we fixed the incident neutron energy at 40.3 meV and used collimations of 60′-20′-42′-44′. We installed a PG filter where appropriate to reduce higher order contamination. The data from each configuration and each sample were normalized to the integrated intensity of the (200) Bragg reflection. All data shown below were collected for the polycrystalline samples at 10 K. However, we also performed room

temperature measurements which demonstrate that there is a negligible contamination of the 10 K data by phonons.

Our principal result is Fig. 3, which shows uncorrected constant $q = 1.1$ Å^{-1} [$= 0.65(2\pi/a)$ where a is the separation between neighboring Ni atoms on the NiO chain] spectra for the pure and 10% Ca doped compounds. For such powder samples, the scans probe the spherically averaged dynamic spin correlation function. The spherical average gives particular weight to the density of states for magnetic excitations near the 1D zone boundary defined by $q = 0.5(2\pi/a)$. Thus, the peak at 9 meV corresponds to the spin gap in the pure compound [6,7]. Ca doping suppresses and smooths the peak, and also introduces substantial spectral weight below the gap. This new weight is entirely magnetic because it disappears upon warming to 300 K or upon increasing q to 3.0 Å^{-1}.

To understand the dramatic effects of Ca doping on the magnetic spectrum, we have examined both a lower doping level, 4%, where two-impurity effects are reduced, and simple chain severing by nonmagnetic Zn^{2+} ions substituted for the $S = 1$ Ni^{2+} ions. Figure 4 shows constant q scans for the four samples studied. Visible states below the gap are clearly unique to the Ca-doped samples. For 4% Ca, they form a narrower band than for 10% Ca. Figure 5 shows constant $\hbar\omega$ scans at 6 and 9 meV. At 9 meV all samples show a steplike onset of scattering for $q > \pi/a$ ($= 0.85$ Å^{-1}) where the lowest energy states in the Haldane spectra become available for scattering. The $\hbar\omega = 6$ meV scans measure the q dependence of the subgap mode. They also reveal a peak at $q = \pi/a$. Thus antiferromagnetic short range order characterizes the states below the gap as it does the Haldane state itself. Even though they yield entirely different behavior below 9 meV, Ca and Zn doping have indistinguishable effects on the scattering above 9 meV. In other words, Ca doping introduces a magnetic degree of freedom which yields new

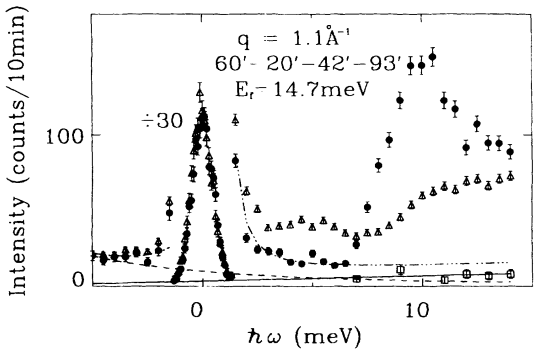

FIG. 3. Constant q scans at $q = 1.1$ Å^{-1} ($0.65a^*$) for Y_2BaNiO_5 (●) and $Y_{1.90}Ca_{0.10}BaNiO_5$ (△) powders at 10 K. Solid line: background measured for analyzer turned 10°. Dashed line: background resulting from $\lambda/2$ neutrons in unfiltered incident beam. Dashed dotted line: tails of elastic ($\hbar\omega = 0$) signal superposed on flat background. Sharp elastic peaks in these raw spectra are due to incoherent nuclear scattering.

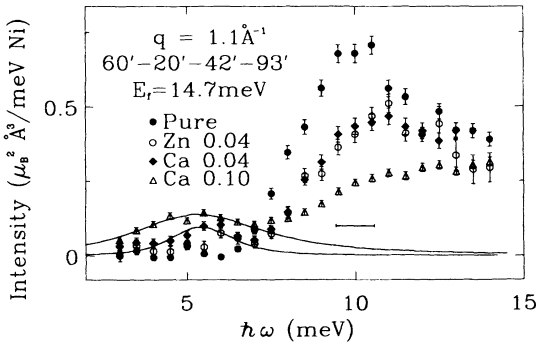

FIG. 4. Normalized constant $q = 1.1$ Å^{-1} scans for Y_2BaNiO_5, $Y_2BaNiO_{0.96}Zn_{0.04}O_5$, $Y_{1.96}Ca_{0.04}BaNiO_5$, and $Y_{1.90}Ca_{0.10}BaNiO_5$ in absolute units. Lines represent fits to the model described in the text. Horizontal bar corresponds to energy resolution (FWHM) at 10 meV. Backgrounds shown in Fig. 3 have been subtracted.

states below the gap and behaves as a chain severing object above the Haldane gap.

The constant q and $\hbar\omega$ scans contain amplitude, energy, and length scales for states introduced into the gap. Constant q scans such as those in Fig. 4 provide energy scales, while the length scales are essentially the inverse widths of the low q edges of the peaks in constant $\hbar\omega$ scans exhibited in Fig. 5. To obtain estimates for the scales, we have modeled the subgap states with the powder average of a simple structure factor. In absence of theoretical guidance, we have chosen a damped harmonic oscillator form with spatial structure factor taken as a Fourier transform of the instantaneous spin correlation function in undiluted integer spin chains [4,17]:

$$S_i^{\perp,\parallel}(q_\parallel,\omega) = \frac{V}{(2\pi)^3}[1+n_\omega] \times \left[1 + 2\sum_{\ell=1}^{\infty}(-1)^\ell e^{-\ell/\xi}\frac{\cos(\ell q_\parallel a)}{\ell^{1/2}}\right] \times \frac{2}{\pi}\frac{\langle m^2\rangle}{3\hbar}\frac{\omega\omega_0\Gamma}{(\omega^2-\omega_0^2)^2+(\omega\Gamma)^2}, \quad (1)$$

where $q_\parallel$ is the component of q along the chain direction, V is the volume per Ni, and n_ω is the Bose factor. We varied the parameters ω_0, Γ, ξ, and $\langle m^2\rangle$ to obtain the best agreement between the powder average of Eq. (1) convolved with the spectrometer resolution function. The solid lines in Figs. 4 and 5(b) represent the outcome of the fitting procedure. While the typical energy $\hbar\omega_0$ did not change appreciably from 5.5 ± 0.3 meV on increasing the Ca content from 4% to 10%, both the effective lifetime Γ^{-1} and correlation length ξ decreased from 10×10^{-13} to 3×10^{-13} sec and from > 10 to 4 ± 1 lattice units, respectively. Thus, the subgap states clearly interact with each other as the typical distance between impurities is reduced. Even so, the spectral weight per impurity, $(1/x)[(2\pi)^3/V]\sum_\alpha \int d^3q\, d\hbar\omega S_i^{\alpha\alpha}(q_\parallel,\omega)$, is $(11.8 \pm 3)\mu_B^2$ for both concentrations of Ca. Identifying the weight with

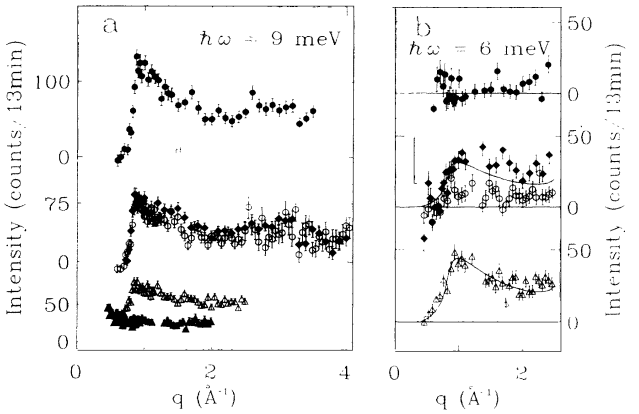

FIG. 5. Normalized constant energy scans for Y_2BaNiO_5, $Y_2BaNi_{0.96}Zn_{0.04}O_5$, $Y_{1.96}Ca_{0.04}BaNiO_5$, and $Y_{1.90}Ca_{0.10}BaNiO_5$. $a^*/2$ is 0.833 25 Å^{-1} for Y_2BaNiO_5. Scans with fixed $E_f = 40.3$ meV and collimations of 60′-20′-42′-44′. Symbols are the same as in Fig. 4. (a) Constant $\hbar\omega = 9$ meV scans. (b) Constant $\hbar\omega = 6$ meV scans. Vertical bar denotes $0.1\mu_B^2$ Å^3/meV/Ni in both (a) and (b). Horizontal bar corresponds to q resolution (FWHM). Filled triangles represent the background as given by the measured count rates at $\hbar\omega = -6$ meV ($\ll k_BT$) for the Ca 0.10 sample.

$g^2S(S+1)\mu_B^2$, we find that for $g = 2$, S lies between 1 and $\frac{3}{2}$, implying that the typical Ca impurity introduces a magnetic disturbance with amplitude substantially larger than that which one might naively associate with a single hole ($S = \frac{1}{2}$).

Our transport data show that Ca doping introduces localized holes onto the NiO chains. Similar to experiments on $La_{2-x}Sr_xCuO_4$ [18] and $La_{2-x}Sr_xNiO_4$ [19], our soft-x-ray absorption spectra on doped Y_2BaNiO_5 show that such holes reside mainly on the oxygen between Ni ions, and will alter the associated superexchange couplings. Thus, if we ignore carrier motion, Ca doping should affect the magnetic dynamics in much the same way as introducing defective springs into a dimerized chain affects its optic phonons: localized states appear below the continuum [20]. Substituting nonmagnetic Zn corresponds to removing atoms and associated springs entirely, and so introduces finite size effects but no fundamentally new states.

In summary, we have discovered that acceptor doping of Y_2BaNiO_5, an insulating NiO chain compound, yields a disordered 1D conductor. The temperature dependent resistivity is of the type associated with variable range hopping in 1D. We have also performed x-ray absorption measurements which show that the carriers reside mainly in the $2p_z$ orbital of the oxygens in the NiO chains. Both O K-edge and Ni L-edge spectra exhibit doping-induced changes for x rays polarized $\parallel a$, but almost no effects when they are polarized $\parallel b$, demonstrating that the carriers are essentially confined to the chains. This result taken together with our transport data clearly make $Y_{2-x}Ca_xBaNiO_5$ the first 1D analog of the doped 2D transition metal oxides. However, in contrast to the latter systems, undoped Y_2BaNiO_5 is not an antiferromagnet, but a compound with a quantum disordered ground state and a Haldane gap in the magnetic excitation spectrum. Therefore, it represents thus far the only quantum spin liquid in any dimension into which carriers can be introduced. Our magnetic neutron scattering measurements reveal that the doped compound no longer contains a simple gapped spin liquid, or even a Haldane state corrected for finite size effects. Instead, carrier doping yields a new phenomenon, namely subgap states which are most simply understood as modes associated with modulation of the superexchange by the holes.

The authors would like to thank B. Batlogg, R. W. Erwin, D. A. Huse, P. B. Littlewood, J. Lynn, J. L. Martinez, and A. P. Ramirez for helpful discussions, H. Y. Hwang for technical assistance, and R. L. Paul for carrying out the neutron activation measurements. C. B. acknowledges support from NSF Grant No. DMR 92302065.

[1] D. B. McWhan *et al.*, Phys. Rev. B **7**, 326 (1973); **7**, 1920 (1973); W. Bao *et al.*, Phys. Rev. Lett. **71**, 766 (1993).
[2] J. G. Bednorz and K. Müller, Z. Phys. B **64**, 189 (1986).
[3] L. F. Mattheiss, Phys. Rev. B **48**, 4532 (1993).
[4] F. D. M. Haldane, Phys. Rev. Lett. **50**, 1153 (1983); W. J. L. Buyers *et al.*, Phys. Rev. Lett. **56**, 371 (1986).
[5] S.-W. Cheong *et al.*, Bull. Am. Phys. Soc. **37**, 116 (1992).
[6] J. Darriet and L. P. Regnault, Solid State Commun. **86**, 409 (1993).
[7] J. F. DiTusa *et al.*, Physica (Amsterdam) **194–196B**, 181 (1994).
[8] B. Batlogg *et al.* (to be published).
[9] D. J. Buttrey *et al.*, J. Solid State Chem. **88**, 291 (1990).
[10] R. Saez-Puche *et al.*, J. Solid State Chem. **93**, 461 (1991).
[11] B. Batlogg *et al.*, Physica (Amsterdam) **194–196B**, 173 (1994).
[12] J. L. Martinez has informed us that his group has also performed such measurements on polycrystalline samples.
[13] P. E. Sulewski (private communication).
[14] See, e.g., O. Madelung, *Introduction to Solid-State Theory* (Springer-Verlag, Berlin, 1978); A. N. Bloch *et al.*, Phys. Rev. Lett. **28**, 753 (1972); P. A. Lee, Phys. Rev. Lett. **53**, 2042 (1984); K. S. Chase, and D. J. Thouless, Phys. Rev. B **39**, 9809 (1989).
[15] D. Kuse and H. R. Zeller, Phys. Rev. Lett. **27**, 1060 (1971); I. F. Shchgolev *et al.*, Pis'ma Eksp. Teor. Fiz. **8**, 353 (1968) [JETP Lett. **8**, 218 (1968)]; L. I. Buravov *et al.*, Pis'ma Zh. Eksp. Teor. Fiz. **12**, 142 (1970) [JETP Lett. **12**, 99 (1970)]; A. B. Fowler, A. Hartstein, and R. A. Webb, Phys. Rev. Lett. **48**, 196 (1982).
[16] C. T. Chen *et al.*, Phys. Rev. Lett. **68**, 2543 (1992); C. T. Chen *et al.*, Phys. Rev. Lett. **66**, 104 (1991).
[17] S. Ma *et al.*, Phys. Rev. Lett. **69**, 3571 (1992).
[18] D. R. Harshman *et al.*, Phys. Rev. B **38**, 852 (1988); A. Aharony *et al.*, Phys. Rev. Lett. **60**, 1330 (1988).
[19] S. M. Hayden *et al.*, Phys. Rev. Lett. **68**, 1061 (1992); Z. Tan *et al.*, Phys. Rev. B **47**, 12 365 (1993), and references therein.
[20] See, e.g., J. M. Ziman, *Principles of the Theory of Solids* (Cambridge University Press, Cambridge, 1972).